

Fabrication and Characterization of Microstacked PZT Actuator for MEMS Applications

Mohd Faizul Mohd Sabri, Takahito Ono, Suhana Mohd Said, Yusuke Kawai, and Masayoshi Esashi

Abstract—A microstacked PZT actuator of dimensions $8\text{ mm} \times 0.8\text{ mm} \times 0.4\text{ mm}$ and capable of $2.3\text{-}\mu\text{m}$ actuation under a voltage of 100 V was fabricated and characterized. This actuator was then integrated into a silicon microstage with dimensions of $20\text{ mm} \times 20\text{ mm} \times 0.4\text{ mm}$ requiring actuation by a miniaturized actuator. The microstage was designed containing a Moonie amplification mechanism in order to further amplify the actuation of the stacked PZT actuator. Experimental characterization of the microstage performance indicated that the combination of a stacked PZT actuator with the Moonie amplification mechanism was successful in enabling high amplification of the microstage to ~ 15 times the original displacement of the PZT actuator. A displacement of $16.5\text{ }\mu\text{m}$ at an applied voltage of 60 V and a resonant frequency of 456 Hz in the lateral vibration mode was observed. The relationship between the actuator parameters and the microstage design and performance was also discussed in order to show that the customized fabrication of a miniature actuator was imperative for the successful design of a high area-efficiency microstage. Analytical derivation of the displacement of the stacked PZT actuator was also carried out in order to evaluate the effectiveness of the fabricated actuator compared with the ideal stacked PZT structure. [2013-0231]

Index Terms—Piezoelectric actuator, silicon stage, micropositioning, amplification mechanism, microelectromechanical systems (MEMS).

I. INTRODUCTION

RAPID DEVELOPMENTS in semiconductor processes have been the driving force in the proliferation of micro and nanoscale devices. The progress in micro and nanoscale devices have rapidly accelerated with corresponding progress in its fabrication methods, such as semiconductor fabrication processes. Micro and nanoscale devices have evolved to a

Manuscript received July 23, 2013; revised March 5, 2014; accepted April 10, 2014. Date of publication May 5, 2014; date of current version January 30, 2015. This work was supported in part by the Cabinet Office, Government of Japan; in part by the Japan Society for the Promotion of Science through the Program for World-Leading Innovative Research and Development on Science and Technology; in part by the High Impact Research Fund Project under Grant UM.C/625/1/HIR/M/OHE/ENG/29; and in part by the Universiti Malaya Research Grant under Grant RP003A-13AET. The work M. F. M. Sabri was supported by the Hitachi Scholarship Foundation. Subject Editor S. M. Spering.

M. F. M. Sabri is with the Department of Mechanical Engineering, Faculty of Engineering, University of Malaya, Kuala Lumpur 50603, Malaysia (e-mail: faizul@um.edu.my).

T. Ono and Y. Kawai are with the Graduate School of Engineering, Tohoku University, Sendai 980-8579, Japan (e-mail: ono@nme.mech.tohoku.ac.jp; kawai@nme.mech.tohoku.ac.jp).

S. M. Said is with the Department of Electrical Engineering, Faculty of Engineering, University of Malaya, Kuala Lumpur 50603, Malaysia (e-mail: ono@nme.mech.tohoku.ac.jp).

M. Esashi is with the Micro System Integration Center, Sendai 980-0845, Japan (e-mail: esashi@mems.mech.tohoku.ac.jp).

Color versions of one or more of the figures in this paper are available online at <http://ieeexplore.ieee.org>.

Digital Object Identifier 10.1109/JMEMS.2014.2317495

sophisticated level, and have contributed to the establishment of nanotechnology as a cutting edge technology in today's world. The applications of nanotechnology have a far-reaching impact in our daily lives, for example, in the form of nanosensors, biomedical devices, data storage devices and scanning probe technology [1]–[6]. One significant family of devices in nanotechnology is the micropositioning device or microstage, which allows translational motion in the microscale. It is a key component in applications where it is crucial to precisely move and manipulate objects, such as in data storage devices [1], [3], optical applications such as micromirror positioning [4], [5], and nanopositioning for biomedical applications [6]. Such systems generally require large actuation strokes with a resolution of the order of nanometers. These actuation strokes also need to be accurate and repeatable. In addition, a high resonant frequency is required for achieving high driving speed for micropositioning. High power density or low driving power is also a concern for the devices, as are size and cost considerations. The degree of miniaturization provided by the microstage is significant, as larger stage dimensions will incur drawbacks such as thermal drift, reduced dynamic performance and larger occupied volume.

The heart of the microstage system is the actuator, as it provides the driving mechanism for translational motion of the stage. The majority of the current microactuator designs utilize electromagnetic or electrostatic actuators. However, each of these actuation methods have their drawbacks. The electrostatic microstage is very low in area efficiency [7]–[9], thus resulting in a large area occupancy by the actuator, instead of the area that can be utilized for translation. Electrostatic actuators also require large driving voltages [7]. The electromagnetic microstage requires the incorporation of a three dimensional coil or the deposition of magnetic materials [10]–[12], hence complicating its fabrication process. In terms of performance, electromagnetic actuators suffer from low operational frequency compared [10]–[12] to other actuation methods such as electrostatic [7]–[9] and piezoelectric actuation [13], [14], due to its material characteristics and the use of a large mass of magnetic material.

This paper presents the fabrication and characterization of a stacked PZT (PbZrTiO_3) actuator which is integrated into a silicon based microstage. A stacked PZT actuator is required in order to optimize the displacement of the actuator, which is notoriously low for a bulk PZT actuator, typically of the order of 0.02% . The choice of piezoelectric actuator results in high operational frequency, fast response, low driving voltage and precise positioning ability [13], [14]. For this work, a miniature PZT actuator was custom-made in order to fit into a compact

microstage containing a Moonie structure. The role of the Moonie structure is to further amplify the inherent displacement of the stacked PZT actuator. The overall emphasis of this investigation is to produce a high area efficiency microstage, where the area efficiency is defined as the ratio of effective area of the moving stage, compared to the total microstage area. As such, minaturisation of the PZT actuator and the inclusion of the Moonie structure are key elements which enable the achievement of a high area efficiency stage. The whole structure is fabricated using standard semiconductor fabrication processes, hence allowing for batch production to reduce cost.

II. THE STACKED PZT ACTUATOR

Piezoelectric ceramics are suitable for actuators, as they possess intrinsic characteristics such as fast response, precise displacement, large force and high operation frequency [4]. Displacement of piezoceramic actuators is mainly dependent on the applied electric field strength E , the length of the actuator L , the forces acting upon it and the properties of the chosen piezoelectric material. The material properties can be characterized by the piezoelectric strain coefficient d_{33} , which describe the relationship between the applied electric field and the resulting mechanical strain.

The change in length, ΔL_o , of an unloaded single-layer piezo actuator can be approximated by

$$\Delta L_o = SL_o \approx \pm Ed_{33}L_o \quad (1)$$

where S is strain (relative length change $\Delta L/L$, dimensionless), L_o is ceramic length, E is electric field strength and d_{33} is the piezoelectric coefficient of the material in the poling direction.

Typically, a bulk PZT actuator as described so far is only capable of 0.02% strain. A strategy to improve the displacement of piezoactuators is to fabricate piezoelectric actuators in a stacked form of alternating piezoelectric material and electrodes, compared to a bulk PZT actuator which is only capable of 0.02% strain. For example, a commercially available stacked piezoceramic actuator by NEC Tokin Co. shows about 0.1% strain [15].

A. Displacement of the Stacked PZT Actuator

The magnitude of displacement for an actuator may be calculated from its dimensions and number of stack layers. If a voltage V is applied to the PZT stack actuator, every single stack layer will respond according to the following equation [15]:

$$\Delta l_i = d_{33}V \quad (2)$$

where Δl_i is the mechanical displacement for a layer, and d_{33} is the piezoelectric coefficient, which is 635×10^{-12} m/V for N-10 type PbZrTiO_3 . Therefore, the total displacement for a particular stacking PZT actuator containing n layers is:

$$\Delta L = \sum_i^n \Delta l_i = nd_{33}V \quad (3)$$

where n is the total number of stack layers. Discussion on the analytical prediction and the experimental performance of

TABLE I
PARAMETERS FOR STIFFNESS AND RESONANCE
FREQUENCY CALCULATION

Material properties (PbZrTiO ₃ , N-10)	
Density	$8.0 \times 10^3 \text{ kg/m}^3$
Piezoelectric coefficient, d_{33}	$635 \times 10^{-12} \text{ m/V}$
Young's modulus	$5.5 \times 10^{10} \text{ N/m}^2$
Permittivity, ϵ_{33}	$4.81 \times 10^{-8} \text{ F/m}$
Frequency constant	1800 Hz-m
Material properties (Ni electrodes)	
Density	8920 kg/m ³
Dimension	0.8×0.4×0.03 mm
Design dimension of stack PZT actuator	
Width, w	0.8 mm
Height, h	0.4 mm
Thickness, t	0.1 mm
Length	8.0 mm
Number of stack, n	58
Stack pitch	0.13 mm
Ni electrodes thickness	0.03 mm

the displacement of the fabricated PZT stacked actuator shall be detailed in Section 5.

The displacement obtained, together with the stiffness of the system, can then be directly used to calculate the blocking force, in Equation (4). The maximum force (blocking force) a piezo actuator can generate depends on its stiffness and maximum displacement, and generated under conditions of infinitely rigid restraint, where its spring constant is infinite.

$$F_{max} \approx k_{Act} \Delta L_o \quad (4)$$

where ΔL_o is maximum nominal displacement without external force or restraint and K_{Act} is piezo actuator stiffness.

In real applications, value of the spring constant of the load may be different from the piezoactuator's spring constant. In this case, the actual force generated by the piezo actuator is:

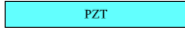
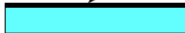

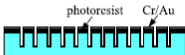

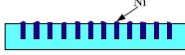



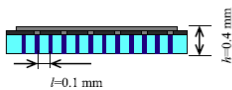
$$F_{max,eff} \approx k_{Act} \Delta L_o \left(1 - \frac{k_{Act}}{k_{Act} - k_S} \right) \quad (5)$$

where k_S is stiffness of external spring.

B. Fabrication of the Stacked PZT Actuator

The stacked PZT actuator was fabricated in-house using Ni electroplating. The in-house fabrication of the PZT actuators was motivated by the fact that the dimensions of the actuator for this microstage design had to be specifically chosen to fit the designed slot for the actuator, and is generally smaller than the commercially available PZT actuators. Precise positioning into the required slot in the microstage would not have been possible using a commercial actuator. In addition, the characteristics of the actuator could be tailored specifically to the requirements of the microstage design, through in-house fabrication of the actuator. For example, the smaller dimensions of the in-house actuator corresponds to an actuator of lower mass, hence enabling a higher resonance frequency for the overall microstage system. The value of the actuation

TABLE II
PROCESS CHART STACKED PZT ACTUATOR FABRICATION PROCESS

Process	Condition/Remark
	Ceramics PZT plate (PbZrTiO₃) Type : N-10 (NEC/Tokin) Size : 40 × 40 × 1 mm
	Photoresist coating OFPR 800 200cp Spin coat : 2000 rpm, Bake : 110 °C, 10 min
	Trench forming - Dicing Blade : NBC-Z 2060 50.8 × 0.002 × 40 Cutting depth : 600 μm, Pitch : 130 μm, Number of trench : 57, Blade rotation : 30000 rpm, Cutting speed : 2 mm/sec, Coolant flow : 0.6 l/min
	Cr/Au deposition - Sputtering (Shibaura sputter) Back-pressure 5×10^{-2} Pa Power - 300 W, Sample rotation - 20 rpm Cr - 50 nm, Au - 200 nm
	Top metal removal - etching MS2001 - 80 °C, 15 min, Rinse 4 times Etacohol Rinse 4 times DI water + Ultrasonic - 20 sec, Spin dry Sidewall metal removal - Dicing Blade : NBC-Z 2060 50.8 × 0.002 × 40 Cutting depth : 500 μm, Blade rotation : 30000 rpm, Cutting speed : 2 mm/sec, Coolant flow : 0.6 l/min
	Nickel electroplating Solution: Ni (NH ₄ SO ₄ H ₂) - 600 g/L, NiCl ₂ ·6H ₂ O - 5 g/L, H ₂ BO ₃ - 40 g/L, CH ₃ (CH ₂) ₃ OSO ₃ Na - 0.2 g/L, C ₂ H ₅ NO ₂ S - 2 g/L, pH : 4.5, Nickel rod 99.999% Ni Current density: Pulse, 30 mA/dm ² , 100 ms at ON, 100 ms at OFF, -50 mA/dm ² , 10 ms at ON Temperature : 55 °C, Time : 250 hours
	Both sides Polishing Load: 800 g, Speed: 30 rpm Swing : 25%-75%, Abrasive : 8 μm
	Polyimide coating (Photoneece UR410) AOP coating - 2000 rpm, 20 sec, bake 90 °C, 1 min, Photoneece UR410 - 1500 rpm, 25 sec, 3000 rpm, 1 sec, bake 80 °C, 90 min, Exposure - 800 mJ/cm ² , Develop - DV605, 8 min (stir), spin dry, Cure in N ₂ Environment 180 °C, 30 min; 270 °C, 30 min; 400 °C, 2 hours
	Cr/Au deposition - Sputtering (Shibaura sputter) Back-pressure 5×10^{-2} Pa Power - 300 W, Sample rotation - 20 rpm Cr - 50 nm, Au - 200 nm
	Photolithography and Cr/Au etching OAP coating - 2000 rpm, 20 sec, bake 90 °C, 1 min, OFPR 200 cp - 2500 rpm, 25 sec, 3000 rpm, 1 sec, bake 90 °C, 30 min, Exposure - 450 mJ/cm ² , Develop - NMD-3, 250 sec, dry spin, Post bake - 110 °C, 10 min Wet etching Au etchant - 10 min, Rinse in DI water 4 times Cr etchant - 3 min, Rinse in DI water 4 times, spin dry

force will also influence the design of the microstage, as will be further elaborated in Section 3.1.

The stacked PZT actuator was fabricated from an N-10 type (NEC/Tokin co. ltd) 1-mm-thick PZT plate. The details of the design parameters and PbZrTiO₃ ceramic properties are shown in Table 1. The 1 mm thick PbZrTiO₃ was first coated with OFPR 200 cp photoresist on its top surface and baked at 110 °C for 1 hour. Later, 600 μm deep grooves with a pitch of 130 μm were produced using a 25 μm thick dicing blade. Cr/Au were then deposited on the top side. At this stage, the metal deposited will act as a seed metal for growing the Nickel electrodes. Therefore, only Cr/Au at the bottom of the trenches are needed and the Cr/Au on top of photoresist and on the trenches walls are removed by removing the photoresist and dicing into the trenches, respectively. Nickel, which functions as the internal electrodes, were then formed in the grooves

using electroplating process. The detailed conditions of the process are shown in Table 2. After polishing both sides of the plate, polyimide was coated and patterned on the top side as an insulator. Next, Cr/Au was deposited and pattern for electrical connection was formed using the photolithography process. The plate was then cut into 8 × 0.8 × 0.4 mm pieces. In total, each miniature actuator contained 58 alternating layers of Ni and PbZrTiO₃. Figure 1 shows the fabricated stacked PZT actuator with interdigitated electrodes connected by Cr/Au pattern.

III. THE SILICON MICROSTAGE

The fabricated actuator was used as a driver for an X-Y translational microstage, with additional amplification provided by a Moonie-type structure [16] as shown

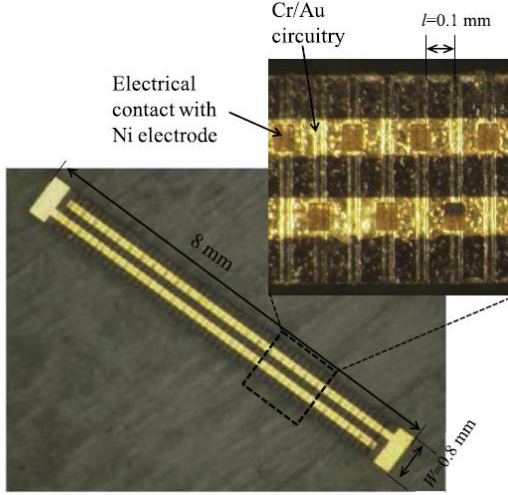


Fig. 1. Photograph of the fabricated ceramics stacked PZT actuator.

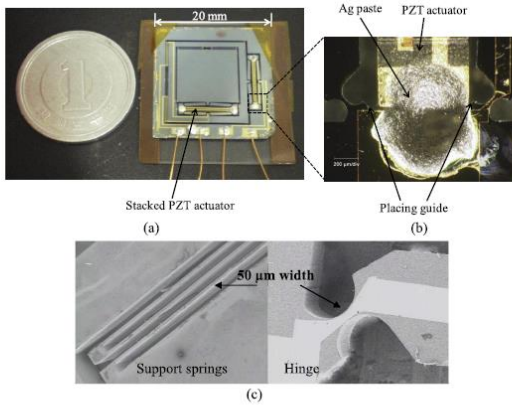


Fig. 2. (a) Photograph of the fabricated silicon stage containing stacked PZT actuators, (b) Photograph showing bonding of actuator with XY microstage by Ag paste, (c) SEM photograph of the support spring and hinge part.

in Figure 2(a). The stage is made from a silicon substrate of dimensions $20 \times 20 \times 0.4$ mm. Silicon is chosen as a base material as it is preferable to metals due to its material properties such as inelasticity, hardness and small thermal expansion. It can also be fabricated using well-developed microfabrication processes. Furthermore, the use of silicon will lower the cost on the basis of batch production.

This design consists of two movable structures arranged so that movement in both the X and Y directions is each controlled by an actuator, as shown in Figure 2(b). The area efficiency is defined as the ratio of the area of the center stage divided by the whole stage area, i.e. the higher this

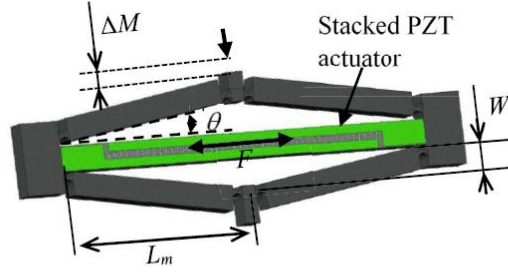


Fig. 3. The principle of Moonie amplification mechanism.

ratio, the higher the microstage area efficiency. A close up of the support springs for the microstage and hinge for the Moonie structure are shown in Figure 2(c). These two components allow flexibility in movement for the microstage, and their dimensions determine the resonant frequency of the microstage. The Moonie structure serves to further amplify the stroke of the stacked PZT microactuator. The center stage is supported by two sets of support beams, and can be actuated by the Moonie amplification mechanism. In addition, the center stage is placed in the movable outer frame, which is also supported by support beams and can be actuated by another Moonie amplification mechanism. The Moonie amplification mechanism is based on four beams arranged in a “diamond” configuration, which is used to drive translation along one axis, as shown in Figure 3. Its basic amplification factor can be calculated by the following equation.

$$R_{AMP} = \frac{L_m}{W} = \frac{\cos \theta}{\sin \theta} = \cot \theta \quad (6)$$

where R_{AMP} is the amplification factor, L_m is the half length of the Moonie mechanism in the expansion direction, W is the half height of the Moonie mechanism and Moonie angle (θ) is the angle of diamond rhombic to the longitudinal direction of the actuator. This equation implies that smaller values of Moonie angle will result in larger amplification factors. Further details of the mechanism of operation for the Moonie structure and microstage fabrication has been discussed in a previous publication [14].

A. Design Considerations for Integrating the Microactuator Into the Microstage

Geometrical matching of the microactuator dimensions, in order to fit into the microstage slot for the microactuator is a key consideration in the design of the microstage, and thus in this case was chosen to be $8 \times 0.8 \times 0.4$ mm. In addition, performance characteristics of the microactuator such as force and actuator mass, have a significant effect on the microstage design. Even though the stacked PZT actuator promises high driving frequency [15], the fundamental frequencies of the stage are limited by its overall design, such as the microstage mass, and restraining forces from friction and support springs. Therefore, it is necessary to predict the resonant frequency of

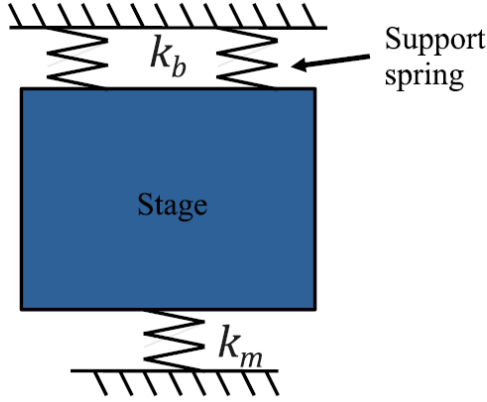


Fig. 4. Simplified spring systems on stage.

the stage, through consideration of stiffness of support springs and hinges.

The close up for the hinge and flexible support beams for the microstage for Figure 2 (c) can be simplified into an equivalent spring system as shown in Figure 4.

In this arrangement, the restoring force of the system is given by

$$F_S = (k_m + k_{b,total})x \quad (7)$$

where stage stiffness

$$k_{Sta} = k_m + k_{b,total} \quad (8)$$

where k_m is the stiffness of Moonie mechanisms and $k_{b,total}$ is the stiffness of support spring [14]. Therefore, the fundamental resonant frequency of in-plane motion is expressed as follows

$$f = \frac{1}{2\pi} \sqrt{\frac{k_{Sta}}{m_{sta,eff}}} \quad (9)$$

where $m_{sta,eff}$ is the effective mass of the moving stage. $m_{sta,eff}$ can be calculated from the volume of the respective parts. Comparison with the experimental performance of the microstage containing the miniature actuator shall be discussed in Section 5.

B. Integration of the Microactuator Into the Microstage

The fabricated actuator was then integrated into the microstage using a dedicated series of microassembly steps, specifically designed for this microstage design as presented in reference [17], [18]. This microassembly strategy will enable reliable and repeatable assembly of this MEMS microstage, and will also set a precedent for the successful microassembly process of similar MEMS devices requiring integration of independently fabricated components. Using this microassembly procedure, integration of a moving part, i.e. in this case the actuator, onto a solid Si substrate is implemented, whilst allowing electrical and mechanical interconnection between the actuator and microstage base. This integration has advantages

TABLE III
PARAMETERS AND CONDITIONS USED IN SIMULATION

Material (Silicon)	properties
Young's modulus	1.9×10^5 MPa
Tensile strength	3.79×10^3 MPa
Density	2.32 g/cm ³
Poisson ratio	0.27
Simulation conditions	
Maximum Element size	0.2 mm
Element type	tetrahedron
Analysis type	3D
Nodes	136735
Number of Elements	22636

over a monolithic fabrication process, which incurs higher production costs and dedicated fabrication processes.

In order to optimize the operation of the miniature actuator in the microstage, simulation of the microstage was carried out, and shall be discussed in the following section.

IV. FEM SIMULATION OF THE MICROSTAGE

A. Simulation Procedure

FEM simulation of the microstage was carried out using ANSYS workbench. The objectives of this simulation are to predict the stage displacement, resonance frequency and amplification factor of the Moonie mechanism. Furthermore, the simulation was also used to identify the parameters of hinges and support springs, which are a function of the maximum force (blocking force) exerted by the actuator. Results of the simulation were then compared with experimental results from the fabricated microstage. Comparison between experiment and simulation results were used to verify the validity of the simulation.

The design of the silicon microstage was used as the basis for FEM simulation, and its volume was divided into a mesh in order to perform finite element analysis on its body. Details of the simulation parameters are shown in Table 3. A loading force from 0 N to 3.5 N, which is in the same order of magnitude exerted by PZT actuators was applied to the Moonie structure. A static solution was obtained in term of overall deformation as a function of the X and Y directions. The simulation results in terms of i) Displacements of the stage as a function of loading force; and ii) Amplification factor as a function of Moonie angle, which shall be discussed in the following section. In addition, modal analysis was performed in order to obtain the resonance frequency of the microstage in the X and Y directions.

B. Simulation Results

1) *Displacement of the XY-Microstage:* The displacement in the X and Y directions were obtained directly from the simulation, as a function of loading force. Figure 5 shows

[Link to Full-Text Articles :](#)

http://ieeexplore.ieee.org/xpls/abs_all.jsp?arnumber=6810136&tag=1